DOI 10.1007/s10717-022-00458-5
Glass and Ceramics, Vol. 79, Nos. 1 – 2, May, 2022 (Russian Original, Nos. 1 – 2, January – February, 2022)

UDC 666.266.6

THE NUCLEATION EFFECT OF PBSE ADDITIVE ON $Bi_2Sr_2CaCu_2O_\delta$ GLASS CERAMICS

Şükrü Çavdar,[1] Emre Deniz,[1] Neslihan Turan,[1, 3] Ahmet Tolga Taşçı,[1] Özgür Öztürk,[2] Haluk Koralay[2]

Abstract published in *Steklo i Keramika*, No. 2, pp. 47 – 48, February, 2022.

Original article submitted March 16, 2021.

The crystallisation kinetics and effects of doping on $Bi_2Sr_2CaCu_2O_\delta$ (BSCCO) glass ceramic system with 0.0%, 0.1%, 0.3% and 0.5% PbSe were investigated in this study. Differential thermal analysis (DTA) was used to investigate the effects of PbSe doping on glass transition, nucleation and crystallisation temperature of glass were investigated. The DTA results were analysed using the Ozawa, Augis–Bennett, Takhor and Kissinger equations for nucleation kinetics to determine the activation energies and Avrami parameters. Thermogravimetric analysis revealed that the amount of oxidation in the structure increased with increasing PbSe-doping concentration.

Keywords: glass, glass ceramics, BSCCO, PbSe, Avrami parameter, DTA/TG.

INTRODUCTION

Glass is an amorphous structure formed by rapid cooling to room temperature of a pure molten mixture of organic and inorganic materials in specific proportions. Glass forms when crystallisation is prevented during this cooling process, and it does not have a fixed melting point. Glass ceramics, in contrast, are polycrystalline materials that are produced when a glass mixture including special components is encouraged to crystallise in a controlled heating process that includes nucleation and crystal growth stages.

Today, glass ceramics are used in many industries because of their characteristics, such as hardness, corrosion resistance and high-temperature durability. Examples of glass-ceramic applications include: nuclear-reactor control rods, radioactive waste regulation and reactor closures, radars for use in outer space, infrared conductors, thermal protectors, biomedical applications, superconducting materials, vacuum technology, high-dielectric-constant materials, and some of the baseplates used in electronics [1 – 8].

Differential thermal analysis (DTA) is one of the most used techniques for the kinetic analysis of glass systems. DTA requires the measurements of the temperature difference of a test material and a reference material heated together in a closed system provides information about the glass transition, crystallisation rate and the activation energy of the system. Changes in the structure can be analysed with different additions and/or substitutions to the structure. The thermogravimetric analysis (TGA) method allows one to analyse values like mass increase (oxidation) and/or mass loss (gas outlet) during the sintering process.

$Bi_2Sr_2CaCu_2O_\delta$ (BSCCO) systems are important superconducting structures. Since these structures can be produced using glass-ceramic techniques, many researchers have prepared glass ceramics with different additives. These studies have improved the understanding of the fundamentals of BSCCO superconductors to make them suitable for technological applications, including terahertz frequency generators, microwave radiation detector, high-velocity logic gates, superconducting quantum interference devices (SQUIDs) and Josephson junctions [9]. Many research groups have analysed the crystallisation mechanisms to improve the superconducting properties of BSCCO systems [10 – 13].

There are many studies in the literature on the use of PbSe as an additive and its low temperature superconducting properties [14 – 16]. In a study on BSCCO glass ceramics, it

[1] Gazi University, Faculty of Sciences, Department of Physics, 06531 Ankara, Turkey.
[2] Department of Electrical and Electronics Engineering, Faculty of Engineering and Architecture, Kastamonu University, 37100 Kastamonu, Turkey.
[3] E-mail: neslihanturan@gazi.edu.tr.

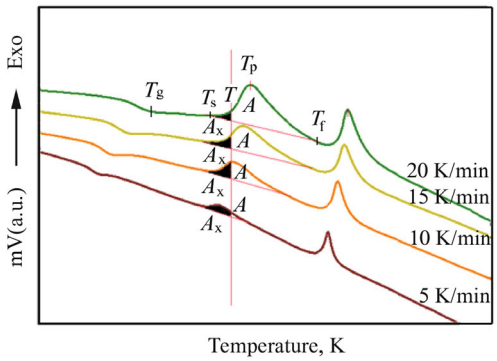

Fig. 1. Typical crystallisation ratio for non-isothermal analysis methods.

was observed that PbSe additive had significant effects on the mechanical properties of the structure [17]. The undoped and PbSe-doped superconducting samples exhibited Indentation size effect behavior and retained their elastic properties, but they were fragile and exhibited the reverse indentation size effect behavior in glass samples. In this study, the changes in the glass structure to the ceramic structure were examined and DTA results were analysed using the Ozawa, Augis–Bennett, Takhor and Kissinger equations for nucleation kinetics to determine the activation energies and Avrami parameters. Thermogravimetric analysis revealed that the amount of oxidation in the structure increased with increasing PbSe-doping concentration.

THEORETICAL BACKGROUND

Activation energy is generally the most important parameter for the crystallisation of amorphous materials. It can be calculated from the energy required for the crystallisation of the samples, the energy required for glass transition and the energy required for melting [18]. Matsushita and Sakka [19] proved that one must consider the mechanism of glass growth to find the crystallisation activation energy. Otherwise, no significant prediction is possible. In this study, the activation energy required for the glass transition is also calculated in addition to the activation energy required for the crystal transition.

Kinematic studies were performed with a differential thermal analyser using the non-isothermal technique. This method provides information about the glass transition temperature and the crystallisation and nucleation mechanisms [20]. The first endothermic peak is referred to as the glass transition temperature (T_g), especially for glass materials, but sometimes this endothermic peak may not appear. In this case, the intersection point of the tangents drawn from the peak side to the starting point is accepted as T_g. The following peaks (T_p) are crystallisation peaks; with some calculations, these peaks provide information about crystallisation, which appears in the form of successive peaks with the increase of the heating rate. At a common temperature value, the crystallisation ratios can be obtained from the areas under the peaks before a certain cut-off. The crystallisation ratio must be calculated separately for each heating-rate analysis [21, 22]. Figure 1 illustrates how to analyse a typical crystallisation peak for non-isothermal analysis.

In Fig. 1, T_a and T_f are the temperatures at which crystallisation begins and ends, respectively, T_p is the crystallisation peak temperature, T is any selected temperature value used to find the crystallisation ratio of the sample, A is the total area under the peak and A_x is the area under the curve between T_a and T [23].

The relation used to calculate the crystallisation rate from the curve obtained with the non-isothermal analysis method is

$$\phi = \frac{A_x}{A}. \tag{1}$$

In the Johnson–Mehl–Avrami equation, the ϕ value is given as

$$\phi(t) = 1 - \exp[-(kt)^n]. \tag{2}$$

Here, ϕ is the conversion rate, k is the reaction rate constant, and n is the Avrami constant.

In order to calculate the size of crystallisation, the Johnson–Mehl–Avrami equation is rearranged as follows [24]:

$$\frac{\mathrm{d}\ln[-\ln(1-\phi)]}{\mathrm{d}\ln\beta} = -n. \tag{3}$$

Here, β is the heating rate and the slope of $\ln[-\ln(1-\phi)]$ versus $\ln\beta$ gives the value of $-n$.

The Avrami parameters obtained from the surface to the inside according to Xie and Gao [25] are as follows:

- $n = 1$: surface nucleation and one-dimensional growth
- $n = 2$: volume nucleation and one-dimensional growth
- $n = 3$: volume nucleation and two-dimensional growth
- $n = 4$: volume nucleation and three-dimensional growth.

Displacements in exothermic peak temperatures, which are the result of the heating rates, are also used in the calculation of the activation energy [26]. The crystallisation activation energy (E_a) was calculated in this study using the Kissinger, Takhor and Augis–Bennett methods, which are based on the Johnson–Mehl–Avrami equation [27]. The activation energies of the samples can be obtained with the Kissinger method using the following equation [28, 29]:

$$\ln(\beta/T_p^2) = -\frac{E_a}{RT_p}. \tag{4}$$

In this equation, E_a is the activation energy and R is the universal gas constant ($R = 8.314\ \mathrm{J \cdot mol^{-1} \cdot K^{-1}}$). The slope of $\ln(\beta/T_p^2)$ versus $1000/T_p$ plot is equal to E_a/R ac-

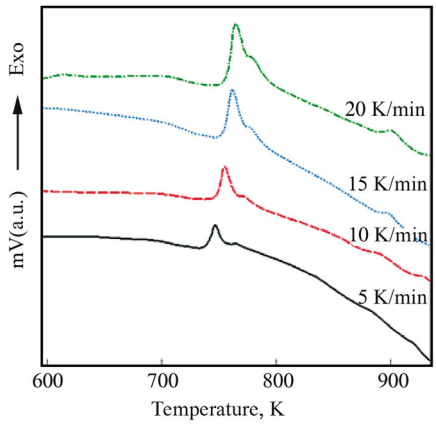

Fig. 2. DTA plots of sample *A* at different heating rates (β = 5, 10, 15 and 20 K/min).

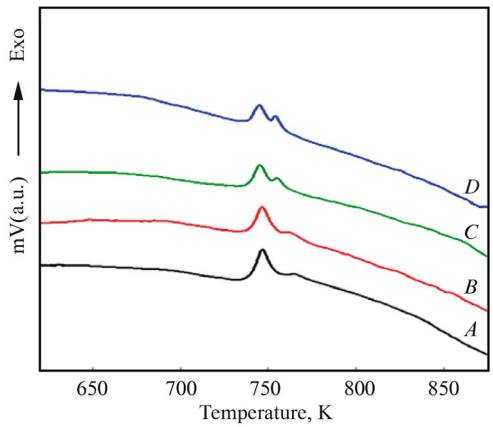

Fig. 3. DTA plots of the samples under an oxygen atmosphere at a 5 K/min heating rate.

cording to the crystallisation-temperature peaks achieved from the DTA curve.

The Takhor method is another method to calculate the activation energy. The activation energy, according to this method, is given by [30]

$$\frac{\mathrm{d}\ln\beta}{\mathrm{d}\ln(1/T_\mathrm{p})}=\frac{E_\mathrm{a}}{R}. \tag{5}$$

Expressions in this equation are the same as in the Kissinger method. From the slope of the ln β versus $(1000/T_\mathrm{p})$ plot, the activation energy can be calculated.

Another alternative method of calculating the activation energy is the Augis–Bennett method. According to this method, the activation energy is given by [31]

$$\frac{\mathrm{d}\ln(\beta/(T_\mathrm{p}-T_0))}{\mathrm{d}(1/T_\mathrm{p})}=-\frac{E_\mathrm{a}}{R}. \tag{6}$$

Here, T_0 is the absolute temperature. The activation energy can be calculated from the slope of ln $(\beta/(T_\mathrm{p}-T_0))$ versus $(1000/T_\mathrm{p})$, as in the other methods.

EXPERIMENTAL PROCEDURE

The preparation of glass ceramics requires detailed information about the crystallisation process of the material. To prepare the samples with a BSCCO composition, high-purity Bi_2O_3, $SrCO_3$, $CaCO_3$, CuO and PbSe chemical powders were mixed in appropriate stoichiometric proportions, in an agate mortar for 1 h at room temperature, until a homogeneous mixture was obtained. The resulting mixture was put into an alumina (α-Al_2O_3) crucible and heated up to 1423 K in a programmable furnace with a 12.5 K/min heating rate. After 1.5-h holding time at this temperature, a molten mixture was obtained. This mixture was poured between two pre-cooled plates. As a result of this rapid cooling procedure, 0.5 – 0.8-mm-thick glass was obtained [17]. Hereafter, we will refer to the resulting samples with 0.0%, 0.1%, 0.3% and 0.5% PbSe additive as samples *A*, *B*, *C* and *D*, respectively.

The SII 7300 EXSTAR thermal analyser was used to take DTA and thermogravimetric measurements from glass samples of approximately 10 mg each. An empty alumina pan was used as the reference sample for non-isothermal DTA tests. The measurements were performed under oxygen gas at four different heating rates.

RESULTS AND DISCUSSION

Differential Thermal Analysis

DTA plots of the undoped sample A measured at β = 5, 10, 15 and 20 K/min are given in Fig. 2. The exothermic peak widths and heights increase and shift towards higher temperatures as the heating rate increases. For instance, the crystallisation temperatures (T_p) for heating rates β = 5, 10, 15 and 20 K/min were 746.7 K, 755.1 K, 762.0 K and 765.0 K, respectively, for sample A. This trend is related to the nucleation rate of the sample. As shown in Fig. 1, the energy required for nucleation will increase more quickly at higher heating rates. Thus, the cross section available for nucleation will decrease. This means that more of the energy required for nucleation is provided at higher temperatures in the crystallisation process. To guarantee sufficient nucleation, the sample must be held at the nucleation temperature for 30 – 120 min. The whole crystallisation process can take up to 5 h in some cases. In order to analyse the variation of the crystallisation peak temperature according to the amount of added PbSe nucleation agent, DTA plots for all samples are shown in Fig. 3. These measurements were taken from samples crystallised with a 5 K/min heating rate. In Fig. 3, while the crystallization peak temperature (T_p) is almost unchanged, the area value under the peaks increases with the nucleation agent added (Table 1). At the same time, the hump-like structure increases significantly with the increase

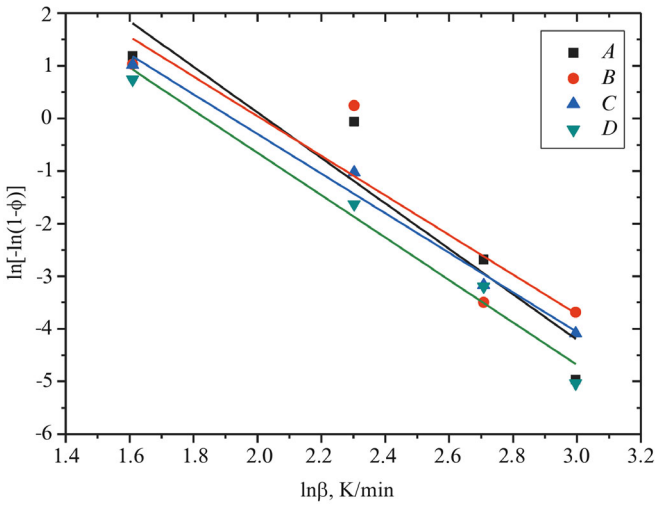

Fig. 4. The plot of ln [–ln (1 – ϕ)] versus ln β for all samples.

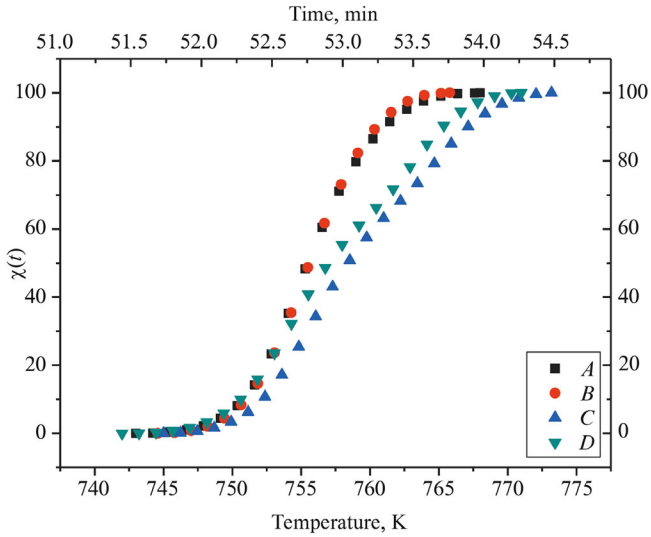

Fig. 5. Crystallised fraction value as a function of temperature and time at a 10 K/min heating rate.

in the added amount of PbSe. It is seen from the DTA plots (Fig. 2) that nucleation is not fully completed at high heating rates, and a hump-like structure appears as the high heating rates. However, for undoped samples, this hump-like structure is only seen with high heating rates. This difference in the results indicates that PbSe affects the glass structure as a catalyser and enables the formation of nucleation sites at lower temperatures. The appearance of the hump-like structure at high heating rates is due to the lack of sufficient time for nucleation [32]. The crystallisation initiation temperature and the peak temperature for sample A were determined as 734.8 – 749.0 K and 746.7 – 765.0 K, respectively. The DTA plots with four different heating rates of all samples from 5 to 20 K/min (Table 1) showed that the crystallisation peak temperatures shifted to higher values with the increase of the heating rate because that the energy needed for crystallisation at lower heating rates was present at lower temperature values. However, the energy necessary for nucleation increased quickly at the higher heating rates.

TABLE 1. Peak Temperature of Crystallisation of Samples at Different Heating Rates

Samples	Heating rate β	T_g	T_s	T_p	A_x	A	$\phi = A_x/A$
A	5	734.8	740.7	746.7	7.560	7.860	0.962
	10	742.5	749.3	755.1	2.720	4.420	0.615
	15	747.8	755.4	762.0	0.510	7.730	0.066
	20	749.0	757.4	765.0	0.100	14.400	0.007
B	5	733.8	740.6	746.7	2.600	2.770	0.939
	10	736.0	749.2	755.3	1.470	5.280	0.278
	15	744.3	755.1	761.9	0.200	6.710	0.030
	20	745.0	759.3	766.2	0.290	11.690	0.025
C	5	734.3	740.6	745.5	3.850	4.110	0.937
	10	741.5	749.4	755.7	1.750	5.790	0.302
	15	744.3	754.1	760.8	0.330	8.020	0.041
	20	747.5	757.8	765.4	0.220	13.220	0.017
D	5	735.5	739.4	745.1	4.940	5.630	0.877
	10	737.8	748.1	754.3	1.650	9.290	0.178
	15	742.7	753.9	760.7	0.640	15.940	0.040
	20	743.8	758.0	766.9	0.110	17.010	0.006

In Fig. 4*a* ln [–ln (1 – ϕ)] versus ln β plot is given for samples *A*, *B*, *C* and *D*. The Avrami parameter can be found from the slope of the curves in Fig. 4, which were plotted using the Ozawa equation [Eq. (3)]. The Avrami parameters were 4.325, 4.037, 3.768 and 3.767 for samples *A*, *B*, *C* and *D*, respectively. According to these values, volume nucleation and three-dimensional growth occurred for samples *A* and *B*, and volume nucleation and two-dimensional growth occurred for samples *C* and *D*. Figure 5 shows the crystallised fraction of the sample as a function of temperature and time at the 10 K/min heating rate. The ranges of temperatures, from initial crystallisation to final temperatures, were 743.0 – 768.0 K, 744.6 – 765.8 K, 745.0 – 773.2 K and 742.0 – 771.0 K for samples *A*, *B*, *C* and *D*, respectively. The crystallisation-temperature range was broader for the samples containing PbSe. The highest temperature range was found with sample *D*; the crystallisation times at a constant heating rate of 10 K/min were 2.64, 2.26, 2.98 and 3.08 min for samples *A*, *B*, *C* and *D*, respectively. Figure 6 shows the crystallisation rate as a function of temperature at a 10 K/min heating rate for all samples. The crystallisation temperature for samples A and B has a single narrow peak, but for samples *C* and *D*, the hump-like structure occurs, and the crystallisation temperature is higher. In Fig. 7, $\ln(\beta/T_p^2)$ was plotted as a function of $1000/T_p$ separately for all samples. This plot allows us to examine the displacements of the exothermic peak temperatures associated with the heating

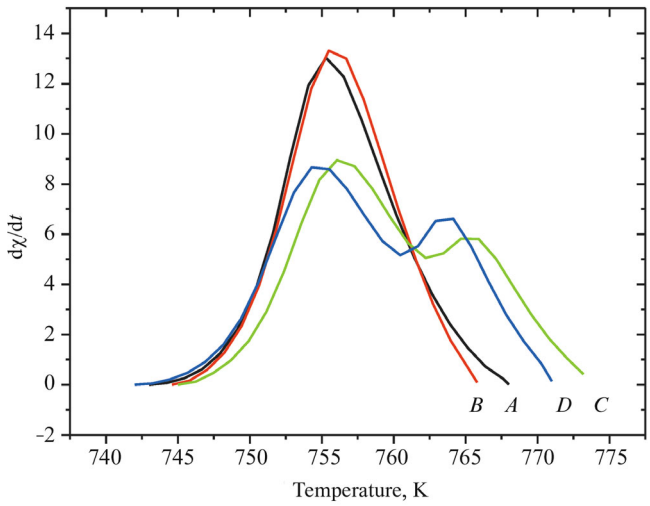

Fig. 6. The crystallisation rate as a function of temperature at a 10 K/min heating rate for all samples.

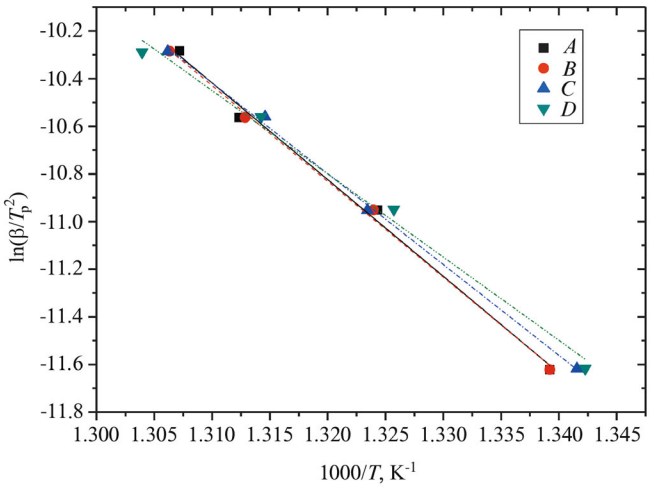

Fig. 7. Plots of $\ln(\beta/T_p^2)$ versus $1000/T_p$ for samples to determine E_a using the Kissinger equation.

rates of the crystallisation process. Activation energies were calculated from the slope of the lines in Fig. 7 using the Kissinger method in Eq. (4). In the same way, activation energies were calculated with the Augis–Bennet and Takhor methods for all samples. The results are consistent for all methods. The results in Table 2 showed that the activation energy was decreased by the PbSe additive. For example, the activation energy of sample *D* was approximately 47 kJ/mol smaller than that of *A*, according to the Kissinger method. The activation energies for samples *A*, *B*, *C* and *D*, calculated using the Kissinger method, were 337.37, 334.24, 316.91 and 290.38 kJ/mol, respectively. These values show that the activation energy decrease with the addition of PbSe. As a result, adding PbSe makes the samples less stable.

Thermogravimetric analysis

The percentile mass variation of the samples with increasing temperature was also determined. TG% measurements were performed under an oxygen flow of 100 ml/min. An increase in the mass of the sample may be caused by oxygen molecules filling the empty unit cells of the BSCCO system, oxidation of some elements or formation of the new crystalline phase. A TG% versus temperature plot of PbSe-doped BSCCO glass with 0%, 0.1%, 0.3% and 0.5% PbSe (*A*, *B*, *C* and *D*) prepared at a 5 K/min heating rate is shown in Fig. 8. The mass gain for all samples began around 900 K and the oxidation process was complete around 1100 K. The total mass gain (Δm), total mass gain per unit temperature ($\Delta m/\Delta T$), total mass gain per unit time ($\Delta m/\Delta t$), total mass gain per unit time per unit oxygen atom $[(\Delta m/\Delta t) \times m_{O_2}]$ and total mass gain per unit temperature per unit oxygen atom $[(\Delta m/\Delta t) \times m_{O_2}]$ were calculated for samples *A*, *B*, *C* and *D* from 5 to 20 K/min at four different

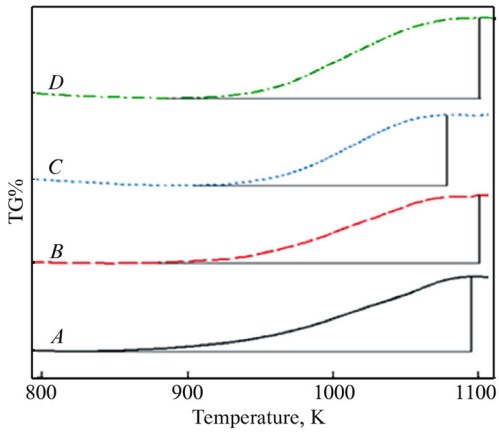

Fig. 8. TG plots of samples under an oxygen atmosphere at a 5 K/min heating rate.

heating rates, and the results are tabulated in Table 3. These results show that with increasing heating rate of an undoped sample, the total mass gain, total mass gain per unit temperature, and total mass gain per unit temperature per unit oxygen atom decrease, whereas the total mass gain per unit time and total mass gain per unit time per unit oxygen atom increase. In general, the total mass gain, total mass gain per unit tem-

TABLE 2. Crystallisation Activation Energies

Activation energy, E_a (kJ/mol) (±0.01)			
Sample	Kissinger method	Takhor method	Augis–Bennett method
A	337.37	349.93	340.09
B	334.24	346.80	336.97
C	316.91	329.47	319.64
D	290.38	302.95	293.11

TABLE 3. Average Oxidation Rates of samples at Different Heating Rates

Heating rate (K/min)	Sample	Total mass increase, Δm (g) ($\pm 0.1 \times 10^{-6}$ g)	Mass increase per temperature ($\Delta m/\Delta T$) ($\pm 0.1 \times 10^{-6}$ g/K)	Mass increase per unit time ($\Delta \mu/\Delta t$) ($\pm 0.1 \times 10^{-6}$ g/sec)	Mass increase per unit O_2 atom ($\Delta m/\Delta t$) × m_{O_2} (atoms/K)	Mass increase per unit O_2 atom and time ($\Delta m/\Delta t$) × m_{O_2} (atoms/sec)
5	*A*	173.78	0.57	2.62	9.07	41.94
	B	82.50	0.41	1.86	6.48	29.72
	C	95.18	0.52	2.40	8.32	38.45
	D	125.00	0.65	2.99	10.43	47.78
10	*A*	160.59	0.58	5.34	9.25	85.38
	B	101.91	0.39	3.56	6.19	57.01
	C	123.95	0.65	6.01	10.45	96.20
	D	150.12	0.69	6.33	10.97	101.26
15	*A*	120.76	0.47	6.47	7.48	103.54
	B	119.29	0.45	6.30	7.26	100.82
	C	121.02	0.58	8.09	9.32	129.49
	D	123.31	0.58	8.01	9.23	128.15
20	*A*	140.66	0.47	8.73	7.47	139.70
	B	133.19	0.39	7.36	6.28	117.82
	C	143.08	0.65	12.08	10.37	193.24
	D	189.95	0.59	11.07	9.47	177.04

perature, total mass gain per unit time, total mass gain per unit time per unit oxygen atom and total mass gain per unit temperature per unit oxygen atom decrease as the heating rate increases for lightly doped samples, but these values increase with higher doping rates.

CONCLUSIONS

In this study, we investigated the crystallisation kinetics and doping effects on PbSe-doped (0.0%, 0.1%, 0.3% and 0.5%) BSCCO glass ceramics. DTA measurements showed that the crystallisation peak temperature was higher at more rapid heating rates. The energy required for crystallisation at a low heating rate is imparted at lower temperatures, whereas at a higher heating rate, the energy required for nucleation is surpassed very quickly, so that crystallisation begins at a higher temperature. The activation energy values for the crystallisation peaks in the DTA curves were calculated for each glass sample using the Kissinger, Augis–Bennet and Takhor methods. The results were consistent across the three methods and showed that increasing the amount of PbSe additive decreased the activation energy of the samples. The TGA results showed that the addition of PbSe increased the oxygen-capture capacity of the samples.

The authors acknowledge financial support for this work through the Scientific Research Projects (BAP 05/2011-48) Foundation of Gazi University Ankara.

REFERENCES

1. L. Yao, G. Chen, T. Yang, Y. Luo, and Y. Yang, "Optical properties and energy transfer in Tb_3 /Sm_3 co-doped Na_2O–CaO–P_2O_5–B_2O_3–ZrO_2 glasses," *J. Alloys Compd.,* **692**, 346 – 350 (2017).
2. H. A. Abo-Mosallam, D. A. Kim, H. W. Kim, and H. H. Lee, "Influence of ZrO_2 oxide on the properties and crystallization of calcium fluoro-aluminosilicate glasses," *Ceram. Int.*, **42**, 4637–5592 (2016).
3. S. Arcaroa, B. Morenob, E. Chinarrob, M. D. Salvadorc, A. Borrellb, M. I. Nietob, R. Morenob, and A. P. Novaes de Oliveiraa, "Properties of LZS/nanoAl_2O_3 glassceramic composites," *J. Alloys Compd.*, **710**, 567 – 574 (2017).
4. G. Peng, D. Zheng, C. Cheng, J. Zhang, and H. Zhang, "Effect of rare-earth addition on morphotropic phase boundary and relaxation behavior of the PNN-PZT ceramics," *J. Alloys Compd.*, **693**, 1250 – 1256 (2017).
5. H. Li, L. Wu, D. Xu, X. Wang, Y. Teng, and Y. Li, "Structure and chemical durability of barium borosilicate glass ceramics containing zirconolite and titanite crystalline phases," *J. Nucl. Mater.*, **466**, 484 – 490 (2015).
6. M. A. Aksan and M. E. Yakinci, "Synthesis and characterization of Er-substituted Bi-2223 H-Tc glass–ceramic superconductors," *J. Alloys Compd.,* **385**, 33 – 43 (2004).
7. A. Polini, H. Bai, and A. P. Tomsia, "Dental applications of nanostructured bioactive glass and its composites," *Nanomed. Nanobiotechnol*., No. 5, 399 – 410 (2013).
8. J. R. Jones, "Review of bioactive glass: from Hench to hybrids," *Acta Biomater.*, No. 9, 4457 – 4486 (2013).
9. D. R. Gulevich, M. Gaifullin, O. E. Kusmartseva, F. V. Kusmartsev, and K. Hirata, "Josephson fluxon pump: theoretical aspects and experimental implementation of elementary flux

quanta generator with BSCCO," *Phys. C: Supercond*., **468**(15 – 20), 1903 – 1906 (2008).
10. O. Kizilaslan and M. A. Aksan, "Crystallization of glass-ceramic $Bi_3Sr_2Ca_2Cu_3O_y$ superconducting system," *J. Cryst. Growth*., **381**, 77 – 82 (2013).
11. Ng. W. Wong, L. P. Cook, and F. Jiang, "Melting equilibria of the Bi–Sr–Ca–Cu–O (BSCCO) system in air: the primary crystallization phase field of the 2212 phase and the effect of silver addition," *J. Am. Ceram. Soc*., **81**(7), 1829 – 1838 (1998).
12. S. S. Ramanathan and L. Zi, K. Ravi-Chandar, "On the growth of BSCCO whiskers," *Phys. C*, **289**, 192 – 198 (1997).
13. X. M. Zhao, T. L. Wang, S. C. Hong, D. L. Sun, N. Wang, G. S. Chae, and Y. Qi, "Superconducting properties and non-isothermal crystallization kinetics of a $Bi_2Sr_2CaCu_2O_8$+d (Bi2212) superconductor prepared by the Pechini sol-gel method," *RSC Adv.*, No. 9, 35280 – 35288 (2019).
14. P. Zolotavin and P. Guyot-Sionnest, "Superconductivity in films of Pb/PbSe core/shell nanocrystals," *ACS Nano*, **6**(9), 8094 – 8104 (2012).
15. L. Andersen, Z. Wang, T. Lorenz, and Y. Ando, "Nematic superconductivity in Cu1.5(PbSe)5(Bi_2Se_3)6," *Phys. Rev. B*, **98**, 220512 (2018).
16. N. Y. Fogel, A. I. Erenburg, A. Pokhila, et al., "Semiconducting chalcogenide multilayers: structure and superconductivity," *Phys. Rev. B*, **284**, 1123 – 1124 (2000).
17. S. Cavdar, E. Deniz, H. Koralay, O. Ozturk, M. Erdem, and A. Gunen, "The effect of PBSE addition on the mechanical properties of Bi-2212 superconductors," *J. Supercond. Nov. Magn.*, **25**, 2297 – 2307 (2012).
18. H. Koralay, S. Cavdar, and M. A. Aksan, "Kinetics of non-isothermal crystallization of Bi3Sr2Ca2Cu3–*x*Sn*x*O10δ glass ceramics," *Physica B*., **405**(23), 4801 – 4805 (2010).
19. K. Matsushita and S. Sakka, "Kinetic study of crystallization of glass by differential thermal analysis–criterion on application of Kissinger plot," *J. Non-Cryst. Solids*, No. 38 – 39, 741 – 746 (1980).
20. O. Kizilaslan, G. Kirat, and M. A. Aksan "Thermal and structural characterization of the $Bi_{2-x}Sm_xSr_2Ca_2Cu_3O_{10+\delta}$ glass-ceramic system," *Int. J. Appl. Glass Sci*., **8**(3), 344 – 351 (2017), doi: 10.1111/ijag.12257.
21. E. B. Araujo, E. Idalgo, A. P. A. Moraes, S. A. G. Filho, and M. J. Filho, "Crystallization kinetics and thermal properties of $20Li_2O – 80TeO_2$ glass," *Mater. Res. Bull.*, **44**, 1596 – 1600 (2009).
22. K. Matusita, K. Takayuki, and Y. Ryosuke, "Kinetics of nonisothermal crystallization process and activation energy for crystal growth in amorphous materials," *J. Mater. Sci.*, **19**, 291 – 296 (1984).
23. A. Goel, E. R. Shaaban, F. C. L. Melo, M. J. Ribeiro, and J. M. F. Ferreira, "Non-isothermal crystallization kinetic studies on $MgO – 114Al_2O_3 – SiO_2 – TiO_2$ glass," *J. Non-Cryst. Solids*, **353**, 169 – 175 (2007).
24. T. Ozawa "Kinetic analysis of derivative curves in thermal analysis," *J. Therm. Anal.*, **2**(3), 301 – 324 (1970).
25. X. Xie and H. Gao, "Calorimetric studies on the crytallization of $Li_2S–B_2O_3$ glasses," *J. Non-Cryst. Solids*, **240**, 166 – 176 (1987).
26. A. Arslan, H. Koralay, Ş. Çavdar, and A. Günen, "Crystallization kinetic studies on $Bi_{1.75}Pb_{0.25}Sr_2Ca_2Cu_{3-x}Sn_xO_\delta$ glass-ceramic by using non-isothermal technique," *J. Non-Cryst. Solids*, **358**, 1190 – 1195 (2012).
27. M. Avrami, "Kinetics of phase changes, 1. General theory," *J. Chem. Phys*., **7**(12), 1103 – 1112 (1939).
28. H. E. Kissinger, "Varition of peak temperature with heating rate in differential thermal analysis," *J. Res. Natl. Bur. Stand*., **57**(4), 217 – 221 (1956).
29. H. E. Kissinger, "Reaction kinetics in differential thermal analysis," *Anal. Chem*., **29**, 1703 (1957).
30. R. L. Takhor, *Advances in Nucleation and Crystallization of Glasses*, The American Ceramics Society (1972), 166 p.
31. J. A. Augis and J. D. Bennett "Calculation of the Avrami parameters for heterogeneous solid state reactions using a modification of the Kissinger method," *J. Therm. Anal*., **13**(2), 283 – 292 (1978).
32. M. A. Aksan, M. E. Yakinci, and Y. Balci, "Thermal analysis study of $Bi_2Sr_2Ca_2Cu_{3-x}Er_xO_{10+\delta}$ glass-ceramic system," *J. Therm. Anal. Calorim.*, **81**, 417 – 423 (2005).